A CATALOGUE OF TAIL FIN SHAPES FOR SMALL WIND TURBINES

K.Kwan, T.Leung, P.Mireault, P.Newman, M.M. Rahman, N.Truong, and D.H. Wood

Department of Mechanical and Manufacturing Engineering

Schulich School of Engineering, University of Calgary, Calgary T2N 1N4, CANADA

1. Introduction

Many small wind turbines use a tail fin to point the rotor into the wind. Fig. 1 shows two typical examples. Rotor alignment is important as average power output decreases by $\cos^2\psi$ where ψ is the yaw angle between the rotor axis and the wind direction, eg Pederson (2004) and Maeda et al. (2008). To maintain high power extraction the tail must follow low frequency wind direction changes, while avoiding high frequency changes. This is because the gyroscopic loads on the blade roots and shaft depend on the yaw rate. For the 500 W turbine design example described in Chapter 9 of Wood (2011), the gyroscopic moment on the generator shaft was the highest load on the turbine, see also Wright & Wood (2007).

Fig. 1: Small wind turbine tail fins. On the left is the Aerogenesis 5 m diameter 5 kW turbine. Above is the 50W Rutland turbine, photo courtesy of KAPEG, Nepal

Since the rotating blades of a wind turbine contribute to yaw stability, Miller (1979) and Bechly et al. (2002), the main purpose of a tail fin is to provide alignment during starting. This can be a challenging requirement because wind direction changes increase in magnitude and frequency as wind speed decreases, e.g. Mahrt (2010) and at sufficiently low wind speed, it is likely that the tail cannot provide the needed restoring moment. Fig. 7 of Wright & Wood (2007) shows a small turbine reaching a yaw angle of 180° when its blades were stationary at a wind speed of 3 m/s.

The two main theories for tail fin response to yaw are the quasi-steady (QS) analysis developed originally for wind vanes, Weiringa (1967), Kristensen (1994), and the unsteady slender body (USB) analysis developed by Ebert & Wood (1995) on the basis of the treatment in Katz & Plotkin (2001). Both have shortcomings: QS ignores the effects of the unsteady wake and the "added mass" of the air that moves with the fin. It appears, however, that the added mass can be ignored for practical tail fin shapes. USB requires the width of the body to vary along the axis to generate steady lift. Thus a rectangular tail fin would experience no steady lift. Both theories are limited to small yaw angles. Nevertheless both are reasonably accurate, at least for delta-shaped tails which are the only ones to have been extensively tested. At a constant wind speed of U m/s with no power extraction, the fin yaws theoretically as a linear second order system. Thus tail fin response can be characterised by the natural frequency, ω_n, and damping ratio, ζ. The two theories predict the same ω_n which is linear in U, but differ in ζ which is independent of U. Ebert & Wood (1995) found that USB gave good estimates for ω_n

and ζ for delta wings with aspect ratio, AR, between 0.7and 3.07for the same tail arm length. The aspect ratio, AR, of any planform is b^2/(planform area) = 2b/c for a delta wing, where b is the span and c is the chord as defined in Fig. 2. Wright (2005) tested a fixed aspect ratio (1.73) delta wing but varied the total yaw inertia, I, for a constant tail arm and then varied the length of the tail arm, x. In the first case, both ω_n and ζ varied as $\sqrt{I}$ as required by QS and USB, but ζ was independent of $\sqrt{I}$ for the second.

The development of tail fin theory in Chapter 8 of Wood (2011) was based on delta wings because their steady lift and drag behaviour is well-known, eg Bertin & Cummings (2009), and they are used in practice, as evidenced by Fig. 1. Ebert & Wood (1995), Wright & Wood (2007), and Wright (2005) all studied delta wings with $x/c < 2$. This work was intended to include other shapes and extend the range of x/c. The turbines in Fig.1 have x/c = 2.1 and 1.1. Nevertheless it would be useful to have additional data at larger x/c.

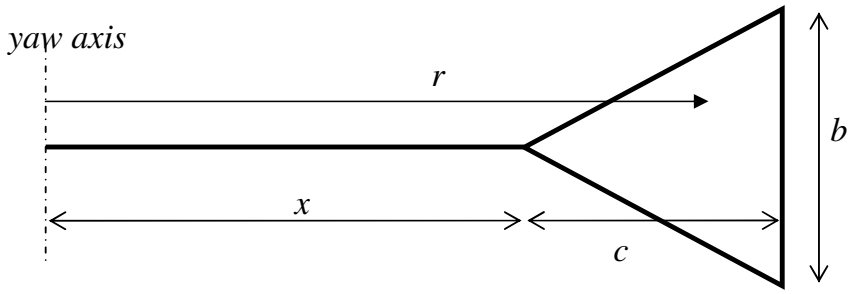

Fig. 2: Basic geometry of a delta wing tail fin. x is the tail armlength, r is the distance from the yaw axis to the centre of pressure, c is the chord,and b is the span

2. Wind Tunnel Tests of Tail Fins

The unidirectional, nominally constant speed wind provided by a wind tunnel is obviously a much simpler environment to study tail fins than a field test of an actual turbine. Both the QS and USB analyses assume small yaw angles and neglect the drag. For a fin in a wind tunnel, the USB yaw response equation is

$$I\ddot{\psi} = K_1\psi + K_2\dot{\psi} + K_3\ddot{\psi} \tag{1}$$

For a delta wing,

$$\begin{aligned} K_1 &= \tfrac{1}{4}\pi\rho b^2U^2(\tfrac{2}{3}c + x) = \tfrac{1}{4}\pi\rho b^2U^2 r, \\ K_2 &= \tfrac{1}{4}\pi\rho b^2U(c+x)^2, \quad \text{and} \\ K_3 &= \tfrac{1}{4}\pi\rho b^2c(c^2/5 + x^2/3 + cx/2), \end{aligned} \tag{2}$$

where ρ is the air density, and the other symbols are defined in Fig. 2, taken from Wood (2011). The K_1 term is the steady lift with the centre of pressure at 2c/3 from the apex and distance r from the yaw axis. K_2 is due to the instantaneous downwash - the trajectory of the flow caused by the lift-produced vorticity. K_3 is the added mass which has been found to be negligible in all cases relevant to tail fins.

(Polhamus, 1966, 1971) derived the following equation for the lift of delta wings:

$$C_L = L\Big/\left(\tfrac{1}{4}\rho U^2 bc\right) = K_p \sin\psi\cos^2\psi + K_v\cos\psi\sin^2\psi \tag{3}$$

where L is the lift, and K_p and K_v depend on the aspect ratio, e.g. Bertin & Cummings (2009). Equation (3) appears to be accurate for delta and other wings for angles up to about 20-30°. At small ψ, the lift is linear in ψ with slope K_p and K_1 in Equation (2) can be written as

$$K_1 = \tfrac{1}{4}\rho b c U^2 C_l r, \quad C_l = \pi b \psi / c \tag{4a}$$

from USB analysis of delta wings or

$$C_l = K_p \psi \tag{4b}$$

from fitting (3) to wind tunnel measurements of delta wings or other planforms. For wind tunnel tests, ω_n for a delta wing tail fin is:

$$\omega_{n,USB} = \sqrt{\frac{K_1}{I + K_3}} \approx \sqrt{\frac{K_1}{I}} \tag{5}$$

and is, therefore, linear in wind speed. The damping ratio is given by

$$\zeta_{USB} = \frac{K_2}{2\sqrt{K_1 (I + K_3)}} \approx \frac{K_2}{2\sqrt{K_1 I}} \tag{6}$$

The approximations in (5) and (6) are valid if the added mass term, K_3, is negligible. The QS analysis leads to the same equation for natural frequency but gives a different damping:

$$\zeta_{USB} / \zeta_{QS} = \left(1 + c/(3r)\right)^2 \tag{7}$$

While the aerodynamics of delta wings is well known, this is not the case for many other shapes that may be used for tail fins. Torres & Mueller (2004) investigated the lift and drag of small-aspect-ratio rectangular plates, ellipses, and similar shapes. There is very little additional useful data and none of non-delta tail fins.

Fig. 3: A delta tail fin in the mid-sectionof the wind tunnel

3. Experimental Set Up and Data Analysis

The experiments were conducted in the 0.76×1.37 m wind tunnel at the University of Calgary shown in Fig. 3. The Pitot-static tube at the left measured U. The uniformity of the mean velocity at the mid-section where the

tail fins were yawed is shown in Fig.4. The variations are significant but are still smaller than the variations and uncertainties in the mean wind speed behind a typical wind turbine. A shaft encoder which resolved to 0.9° was connected to the underneath section of the vertical shaft to measure ψ. Particular care was taken to minimize the friction in the two bearings holding the vertical shaft and it was determined that the remaining friction did not influence the yaw response.

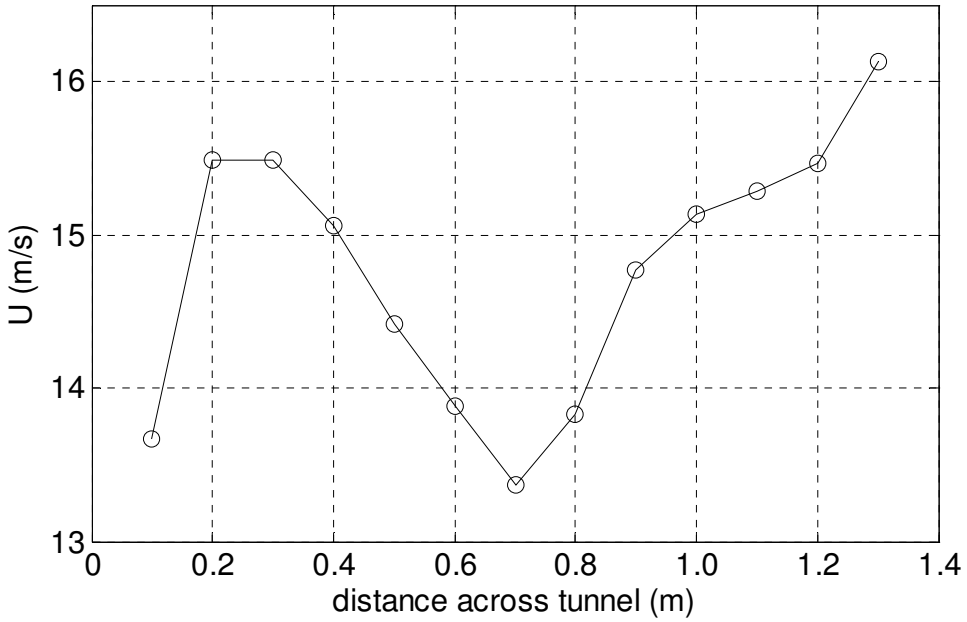

Fig. 4: Mean velocity across the mid-section of the wind tunnel. The vertical shaft of the tail fin was mounted at 0.7m.

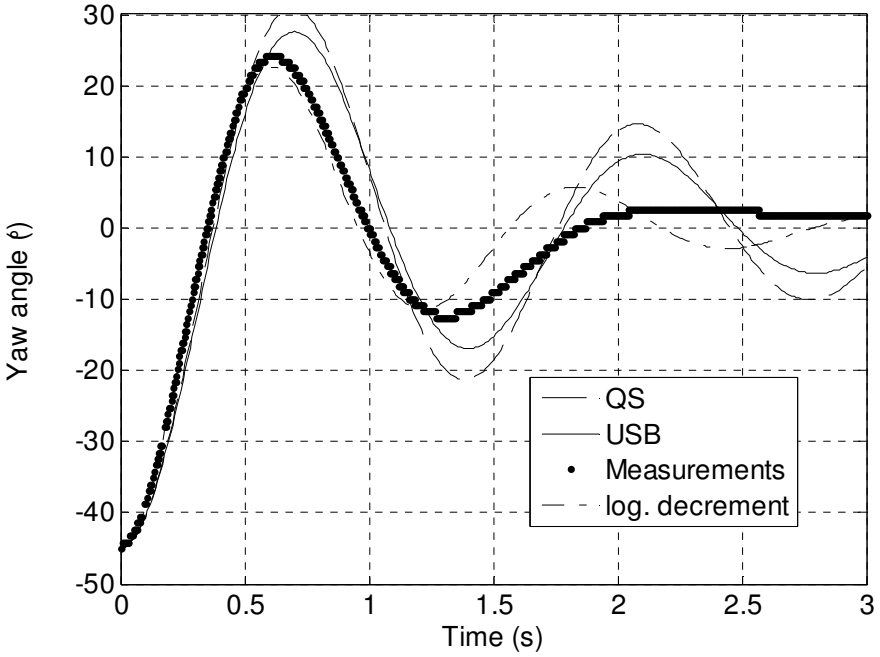

Fig. 5: Measured and predicted response of delta wing with AR = 0.58. Only one set of measurements is shown

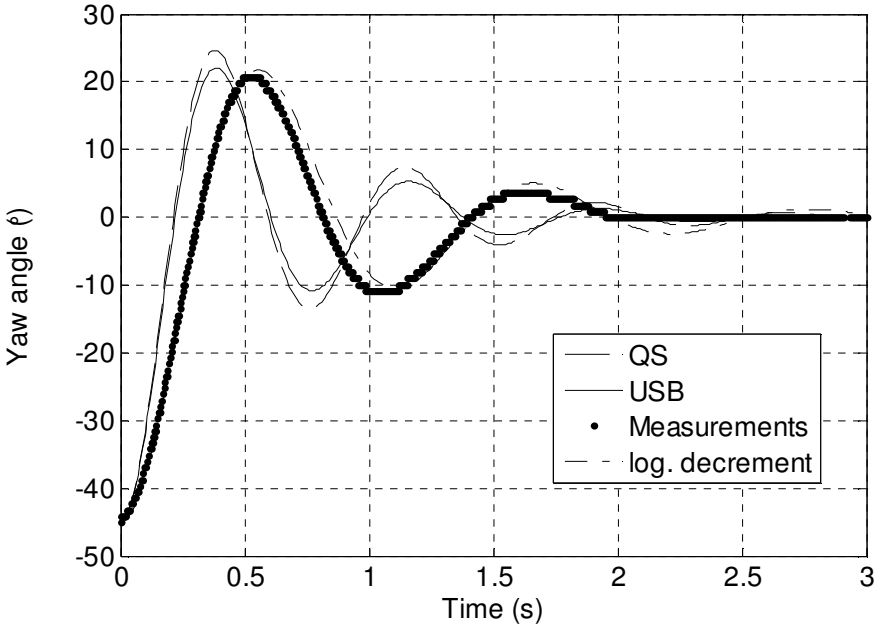

Fig. 6: Measured and predicted response of delta wing with AR = 1.97. Only one set of measurements is shown

Table A1 in the Appendix documents the geometries and ARs tested and the tail fin inertia, I_t. The vertical shaft and tail arm, used for all tests, had a combined inertia I_a, of 1.501×10^{-2} kgm^2. x was 0.447 m for all tests.. The inertia, I, in Equations (5) and (6) is given by $I = I_a + I_t$.

Figs. 5 and 6 show typical tests. The fin was released from an angle of 45° and its subsequent motion recorded. The effects of the encoder resolution are clearly visible at the larger times. Each tail fin was tested ten times but only one result is shown in Figs. 5 and 6. It was necessary to use a high release angle to generate accurate data and there was no evidence that this induced any non-linearities in the response. The reproducibility of the tests was generally very good. However, it proved surprisingly difficult to devise a simple and accurate method of determining ω_n, and ζ. The two best methods proved to be the logarithmic decrement method and the measurement of the maximum positive peak (y_{max}). The fitted logarithmic decrement response is plotted in the following figures. On the scale of the figures, it was indistinguishably different from the y_{max} response.

4. Results and Discussion

Tables 1- 4 summarize the natural frequency, damping ratio, and their standard deviations for the range of shapes and aspect ratios tested. In USB, delta wings behave identically to right triangles. It is clear that there are no significant variations in ω_n and ζ between the two geometries. In general, there is remarkably little variation over the entire range of geometries. Figs. 4 and 5 suggest that both theories are more accurate at low AR where the damping is under-estimated, but over-estimate the natural frequency at higher AR,

Table 1: Damping Ratio and Natural Frequency for Delta Wings at U = 12.1 m/s

AR	Average ζ from log decrement	Std Dev.	Average ζ from y_{max}	Std Dev.	Average ω_n from log decrement (rad/s)	Std Dev. (rad/s)	Average ω_n from y_{max} (rad/s)	Std Dev. (rad/s)
0.578	0.214	0.008	0.204	0.008	5.28	0.19	5.24	0.21
1.01	0.210	0.006	0.209	0.011	5.63	0.25	5.63	0.27
1.52	0.218	0.016	0.219	0.011	5.75	0.27	5.75	0.29
1.97	0.226	0.011	0.247	0.013	5.83	0.23	5.93	0.22
2.5	0.224	0.011	0.257	0.014	5.53	0.29	5.68	0.28

Table 2: Damping Ratio and Natural Frequency for Right Triangles at U = 12.1 m/s

AR	Average ζ from log decrement	Std Dev.	Average ζ from y_{max}	Std Dev.	Average ω_n from log decrement (rad/s)	Std Dev. (rad/s)	Average ω_n from y_{max} (rad/s)	Std Dev. (rad/s)
0.522	0.218	0.006	0.203	0.006	5.19	0.11	5.13	0.11
0.796	0.218	0.010	0.231	0.010	5.24	0.18	5.30	0.19
1.08	0.225	0.015	0.240	0.012	5.46	0.28	5.53	0.25
1.50	0.230	0.013	0.252	0.011	5.43	0.19	5.53	0.16
1.99	0.244	0.014	0.256	0.008	5.50	0.27	5.55	0.27

Table 3: Damping Ratio and Natural Frequency for Rectangles at U = 12.1m/s

AR	Average ζ from log decrement	Std Dev.	Average ζ from y_{max}	Std Dev.	Average ω_n from log decrement (rad/s)	Std Dev. (rad/s)	Average ω_n from y_{max} (rad/s)	Std Dev. (rad/s)
0.507	0.196	0.011	0.185	0.010	5.65	0.25	5.60	0.25
0.990	0.206	0.009	0.234	0.011	5.34	0.25	5.46	0.24
1.45	0.222	0.009	0.239	0.009	5.67	0.26	5.74	0.24
2.03	0.235	0.008	0.256	0.010	5.24	0.25	5.32	0.26
2.42	0.229	0.017	0.266	0.011	5.38	0.19	5.55	0.23

Table 4: Damping Ratio and Natural Frequency for Ellipses at U = 12.0 m/s

AR	Average ζ from log decrement	Std Dev.	Average ζ from y_{max}	Std Dev.	Average ω_n from log decrement (rad/s)	Std Dev. (rad/s)	Average ω_n from y_{max} (rad/s)	Std Dev. (rad/s)
0.495	0.173	0.010	0.184	0.009	5.21	0.21	5.25	0.22
1.62	0.200	0.008	0.232	0.006	5.10	0.14	5.24	0.16
1.99	0.212	0.009	0.241	0.014	5.13	0.24	5.26	0.26
2.51	0.225	0.010	0.252	0.007	5.01	0.25	5.12	0.23

The indivdual results in Figs. 5 and 6 show very little difference in the predicted ω_n between the two theories. This is because the added mass term, which appears in USB but not in QS, is small. Table 5 shows the calculated constants in Eq. (2) for the delta wings. Comparison with the table in the Appendix shows that K_3 can be neglected in comparison to the inertia.

Table 5: Constants in Eq. (2) for the delta wings tested.

AR	K_1 (kgm^2/s^2)	K_2 (kgm^2/s)	K_3 (kgm^2) x10^{-4}
0.578	0.5624	0.0357	2.19
1.01	0.8169	0.0487	2.29
1.52	1.159	0.0640	2.50
1.97	1.488	0.0789	2.75
2.5	1.883	0.0969	3.07

Since about half the turbine yaw inertia can be due to the blades and other components, Wood (2011), it is

useful to present the results in manner that eliminates *I*. One possible way is seen in Fig. 7 which compares all the available data to the two theories. (Fig. 7 and subsequent figures show ω_n and ζ from the log decrement determination.) Interestingly the natural frequency-damping ratio, which is related to the ratio of the second to first derivative in the governing differential equation, is also independent of the AR. USB provides a better approximation to the results than QS but not by much. The line of fit

$$\omega_n c/(\zeta U) \;=\; 0.93\exp(-0.28\,x/c) \tag{8}$$

appears to be a good first approximation for all shapes. Fig. 8 shows the reduced frequency[1], $\omega_n c/U$ against *x*/*c*. The error bars show the standard deviation from Tables 1 – 4. The collapse is apparently better than shown in Fig. 7 suggesting that ζ should also be independent *I*. The line

$$\omega_n c/U \;=\; 0.11\exp\left[-0.09\left(x/c\right)^{2.2}\right] + 0.03 \tag{9}$$

approximately fits the data for all shapes over the range of *x*/*c*. Fig. 9 displays all measurements of ζ against *x*/*c* with the error bars indicating the standard deviation from Tables 1 – 4. The collapse is not as good as in Fig. 8 probably for two related reasons: first ζ is more difficult to determine accurately and the evidence for its scaling is contradictory. For example, Fig. 3 of Ebert & Wood (1995) suggests that ζ is independent of *x*/*c*, whereas Fig.2.12 of Wright (2005) shows ζ is proportional to $\sqrt{I}$ as it changes with *x*/*c*, at least over a limited range of ζ. However, Wright's (2005) Fig. 2.14 suggests that ζ is independent of $\sqrt{I}$ when varied by changing *x*. It follows from Equations (2) and (6) that $\zeta \sim x/c$ at large *x*/*c* if *I* is unimportant and the data is consistent with this, but it is not clear whether the present delta wing and right triangle data legitimately behave differently from the other shapes and from the obvious extrapolation of the previous delta wing data.

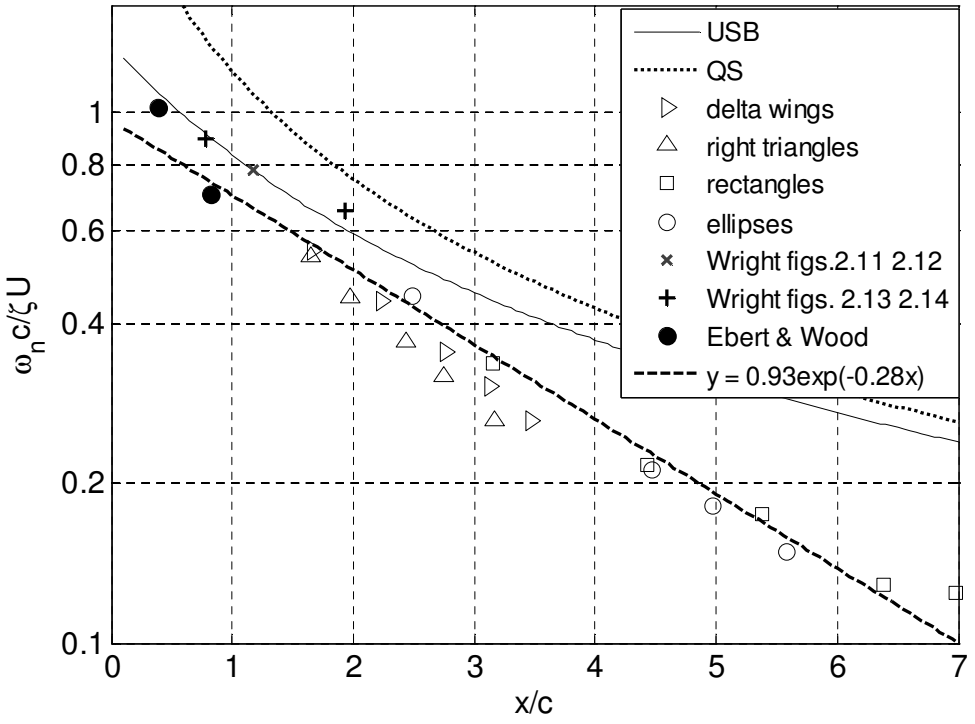

Fig. 7: The natural frequency- damping ratio for all shapes

[1] In unsteady aerodynamics the reduced frequency is usually defined as $fc/(2U)$ where *f* is the frequency in Hz. The present definition is more useful for tail fin studies.

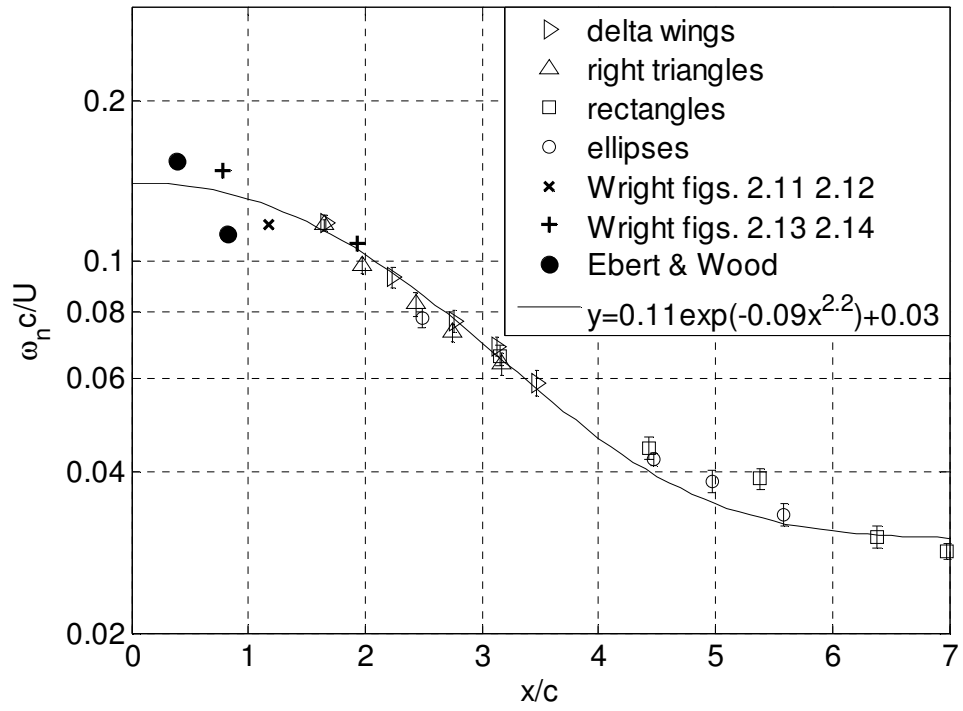

Fig. 8: The natural frequency for all shapes

Finally, Fig. 10 shows the behaviour of $\zeta\sqrt{I}$. These results also suggest a larger difference in behaviour between delta wings and right triangles and the other two geometries than does Fig. 8. Fig. 9 suggests that the first two give a higher damping for the same inertia, but the limited data must be treated with caution partly because Wright's (2005) Fig. 2.12 results for delta wings has $\zeta\sqrt{I}$ = 0.0077, that is mid-way between the two sets of the present results.

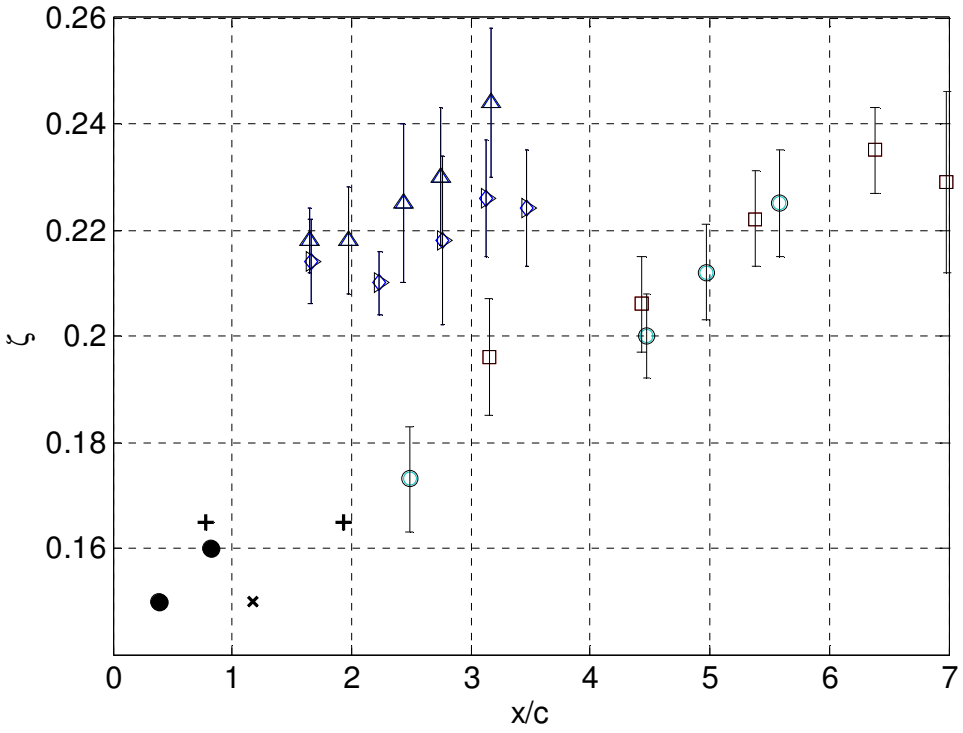

Fig. 9: The damping ratio for all shapes. Symbols as in Fig. 8.

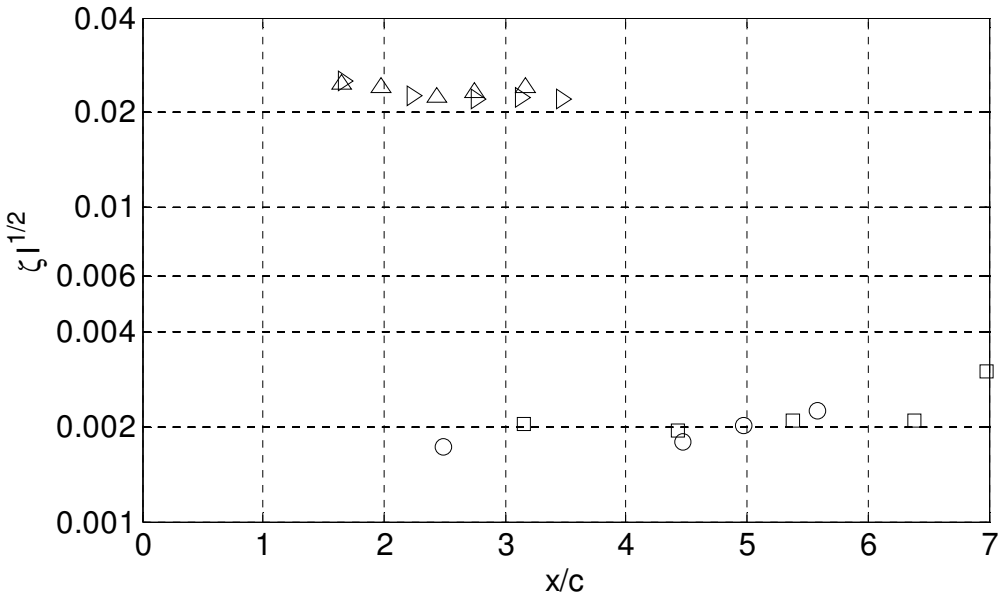

Fig. 10: The product of damping ratio and square root inertia for all shapes. Symbols as in Fig.8.

5. Conclusions

The data presented in this paper show the effect of tail fin shape and arm length on the natural frequency and damping ratio that characterize tail fin behaviour in yaw. The data also significantly extend the available range of the ratio of the distance to the yaw axis to chord length so that all values used in practice should now be covered. The two main descriptions of tail fin yaw response, unsteady slender body theory and the quasi-steady analysis explain some, but not all the features of the response. In particular the tail fin reduced frequency for all shapes scaled approximately with the normalized distance to the yaw axis which, if generally true, represents a simpler behaviour than allowed by both theories. It suggests that tail fin planform only has a small impact on the yaw behaviour.

For the damping ratio, the situation is less clear, apart from the obvious general increase with normalized distance. It appears that delta wings and right triangles have higher damping than rectangles and ellipses but the difference is small, not much larger than the standard deviation in the measurements and within the differences between the two methods used to estimate the damping ratio.

Acknowledgments

This work is part of a program supported by the National Science and Engineering Research Council, the ENMAX Corporation, and the Schulich endowment to the University of Calgary. The mean velocity data in Fig.4 was obtained by Xavier Ortiz.

5. References

Bechly M.E., Gutierrez H., Streiner S., Wood, D.H., 2002. Modelling the Yaw Behaviour of Small Wind Turbines, Wind Engineering, 26, 223-239.

Bertin J, Cummings R (2009) Aerodynamics for Engineers. Pearson Prentice Hall, 5th edition

Ebert, P.R., Wood D.H., 1995. On the Dynamics of Tail Fins and Wind Vanes. Journal of Wind Engineering and Industrial Aerodynamics 56**,** 137-158.

Katz J., Plotkin A., 2001. Low Speed Aerodynamics: 2nd edition, Cambridge.

Kristensen, L., 1994. Cups, Props and Vanes, Riso National Laboratory, Roskilde, Denmark, http://www.risoe.dk/rispubl/VEA/ris-r-766.htm (accessed 21 May. 2011)

Maeda, T., Kamada, Y., Suzuki, J., Fujioka, H., 2008. Performance Under Yawed Inflow. Journal of Solar Energy Engineering, 130, 1 – 7.

Mahrt, L. 2010. Surface wind direction variability, J. Appl. Meteorol Climatol, 50, 144 – 152.

Miller, R.H.,1979. On the weathervaning of wind turbines. J. Energy, 4, 319 – 320.

Pedersen, T.,2004. On Wind Turbine Power Performance Measurements at Inclined Airflow, Wind Energy, 7, 163 – 174.
Polhamus, E.C., 1966). A concept of the vortex lift of sharp-edge delta wings based on a leading-edge suction analogy. NASA TN D-3767, December 1966.
Polhamus, E.C., 1971.Predictions of Vortex-Lift Characteristics by a Leading-Edge Suction Analogy. Journal of Aircraft, 8; 193-199.
Torres, G.E., Mueller, T.J., 2004. Low aspect ratio aerodynamics at low Reynolds numbers. AIAA Journal, 42; 865 – 873.
Weiringa, J., 1967. Evaluation and Design of Wind Vanes. Journal of Applied Meteorology, 6, 1114-1122.
Wood, D.H. 2011. Small Wind Turbines:Analysis, Design,and Application, Spribker.
Wright, A. D, Wood, D. H., 2007. Yaw rate, rotor speed and gyroscopic loads on a small horizontal-axis wind turbine, Wind Engineering, 31, 197 – 209.
Wright, AK (2005) Aspects of the Aerodynamics and Operation of a Small Horizontal Axis Wind Turbine. PhD thesis, School of Engineering, University of Newcastle.

Appendix: Properties of the Tail Fins

All fins were made from 16 gauge Aluminium with an average thickness of 1.2 mm. I was calculated from the following formulae:

For Delta Wings and Right Triangles:

$$I_t = m\left[x^2 + c^2/2 + 4xc/3 \right] \tag{A1}$$

For Rectangles:

$$I_t = m\left[x^2 + c^2/3 + xc \right] \tag{A2}$$

and for Ellipses:

$$I_t = m\left[x^2 + 5c^2/16 + xc \right] \tag{A3}$$

Table A1: Tail fin geometries

Tail Fin Shape	AR	b (mm)	c (mm)	Measured mass (g)	I_t (kgm^2)×10^{-2}
Delta wing	0.578	78	270	34.63	1.389
	1.01	101	200	32.82	1.146
	1.52	123	162	32.58	1.016
	1.97	141	143	33.16	0.9725
	2.5	160	129		0.9768
Right Triangles	0.522	71	272	32.38	1.279
	0.796	90	226	32.79	1.216
	1.08	99	184	29.23	0.9873
	1.50	122	163	32.09	1.024
	1.99	140	141	31.84	0.9630
Rectangles	0.507	72	142		0.8994
	0.990	100	101		0.4412
	1.45	120	83		0.4149
	2.03	142	70		0.4057
	2.42	155	64		0.3944
Ellipses	0.495	70	180		0.5928
	1.62	122	100		0.4894
	1.99	141	90		0.4987
	2.51	158	80		0.4865